Astronautica Acta. Vol. 18, pp. 171–184. Pergamon Press 1973. Printed in Great Britain

Normal and Tangential Momentum Accommodation for Earth Satellite Conditions

Earl D. Knechtel and William C. Pitts

Research Scientists, Ames Research Center, NASA, Moffett Field, California, 94035, U.S.A.

(*Received* 10 *January* 1972)

Abstract—Normal and Tangential Momentum Accommodation for Earth Satellite Conditions. Momentum accommodation was determined experimentally for gas-surface interactions simulating in a practical way those of near-earth satellites. Throughout the ranges of gas energies and incidence angles of interest for earth-conditions, two components of force were measured by means of a vacuum microbalance to determine the normal and tangential momentum-accommodation coefficients for nitrogen ions on technical-quality aluminum surfaces. For these experimental conditions, the electrodynamics of ion neutralization near the surface indicate that results for nitrogen ions should differ relatively little from those for nitrogen molecules, which comprise the largest component of momentum flux for near-earth satellites.

The experimental results indicated that both normal and tangential momentum-accommodation coefficients varied widely with energy, tending to be relatively well accommodated at the higher energies, but becoming progressively less accommodated as the energy was reduced to and below that for earth-satellite speeds. Both coefficients also varied greatly with incidence angle, the normal momentum becoming less accommodated as the incidence angle became more glancing, whereas the tangential momentum generally became more fully accommodated. For each momentum coefficient, an empirical correlation function was obtained which closely approximated the experimental results over the ranges of energy and incidence angle. Most of the observed variations of momentum accommodation with energy and incidence angle were qualitatively indicated by a calculation using a three-dimensional model that simulated the target surface by a one-dimensional attractive potential and hard sphere reflectors.

Translated abstracts appear at the end of this article.

Introduction

THE DEVELOPMENT and increased use of earth satellites during the past decade or more have caused additional emphasis on the relatively old problem of momentum exchange between free-molecular gas flows and the surfaces on which they impinge. A number of comprehensive studies [1, 2, 3] have summarized the historical background and physical reasoning that led to the formulation by Knudsen, Maxwell, Schaaf and others of the dimensionless accommodation coefficients conventionally employed in the study of gas-surface interactions. Although significant advances have been made in both theoretical and experimental methods in recent years, a recent comprehensive literature survey [4] indicates that very few experimental results are available which satisfactorily simulate earth-satellite conditions with respect to the major variables. For example, of 201 gas-surface interaction papers reviewed in Ref. 4, scarcely 10% were at or near the proper range of gas energies for satellites. In addition, there are often other severe limitations regarding the gas species, the type and condition of the surface, the range of incidence angles, and the adequacy of the measured data for application to earth satellites.

In gas-surface interaction research related to satellites, the major emphasis initially has been on the degree of momentum accommodation and how it affects satellite drag and orbital lifetime. Experiments planned only for these purposes may be somewhat simplified by measuring only the drag component of force on the surface, as was the case in Refs. 5, 6, and 7. However, it is often required to calculate not only the drag of orbiting bodies but their asymmetric torques as well. The latter situation requires knowledge of both the normal and tangential momentum accommodation and, as indicated in Ref. 8, is becoming relatively more important for the larger and longer-lived satellites.

The present experimental study therefore was designed to provide needed data of this more general type, simulating to a practical degree the conditions of near-earth satellites as well as facilitating comparison

[1] Presented at the XXII Int'l Astronautical Congress of the IAF, Brussels, Belgium, Sept. 20–25, 1971.

with other results using conventional normal and tangential momentum-accommodation coefficients. These coefficients were determined from the measured lift and drag on aluminum surfaces and the measured properties of the impinging ion beam.

The results of Ref. 9 indicated, for argon ions incident on both gold and aluminum surfaces, some consistent variations of the momentum-accommodation coefficients with the energy and incidence angle of the gas particles. The variations confirmed some earlier conclusions [10] which had been inferred from measured drag of spheres in a highly rarefied flow. The present work has extended in several ways that of Ref. 9. First, the gas species was changed to nitrogen which makes the major momentum contribution for satellite attitudes up to about 300 km. Also, the ion gun was redesigned and the experimental methods improved to permit more precise measurements down to energies completely through the range of interest for earth satellites as well as over a wider range of incidence angles.

Practical compromises were made in two respects which lessened the experimental difficulties. These were first, in not attempting to test ultraclean surfaces and second, by using an ion beam rather than the much more difficult molecular beam. In both cases, simple analyses were made which appear to justify these approaches to realistic simulation of gas-surface interactions for near-earth satellites.

Experimental Apparatus

The test facility used for the present experiment is shown in Fig. 1. The major components include the vacuum microbalance chamber at the top, the hexagonal test chamber with an ion source attached to its lower surface, and two pump assemblies (only one pump visible in figure). A typical target is shown suspended from the balance in test position. Also shown on one wall of the test section are two axial and rotary-motion manipulator shafts that permit ion probes and targets to be moved into and out of the ion beam while it is in operation.

Figure 2 shows the ion-beam source with one of three alternate tungsten filament cathodes. The anode was segmented to ensure maximum plasma density at the point of ion extraction. Conical baffles were placed in the auxiliary anode to capture contaminants created in the cathode housing.

The ion source was operated in a glow discharge mode. To maintain this condition it was necessary to maintain the pressure in the discharge region within certain limits that were of the order of 10^{-3} torr. Because it was desired to keep the pressure in the test chamber as low as possible, the ion beam was extracted from the glow discharge through a narrow slit. The proper pressure levels were obtained by balancing the input gas rate with the speed of the diffusion pumps. The operating gas was N_2 for the test, but a wide variety of gases could be used in the system.

There were several reasons for turning the ion beam 90° after extraction from the anode region. One was for further insurance that contaminants from the cathode housing region did not reach the targets. The primary reasons concerned the differential pressure between the ion source and the test chamber. Because of this differential pressure, there was a steady flow

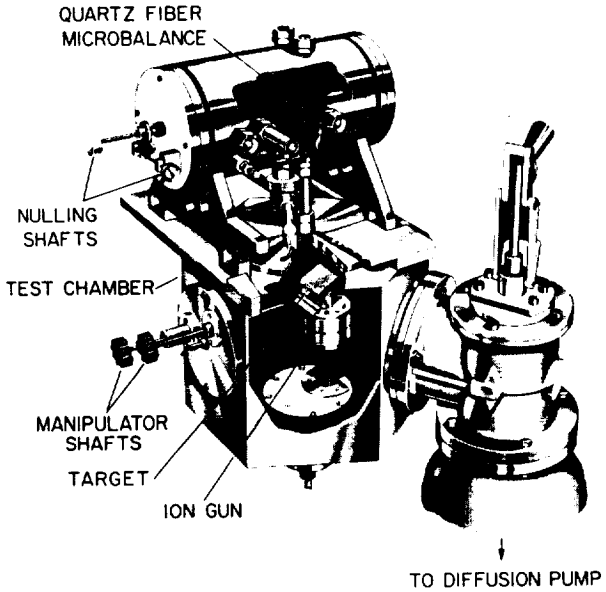

FIG. 1. Cutaway view of ion-beam facility.

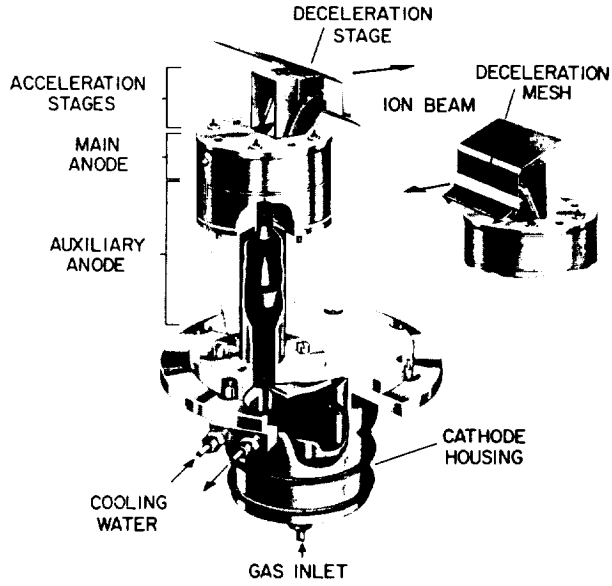

FIG. 2. Cutaway view of ion source.

of background gas through the beam extraction slit that would have caused, a large tare force on the targets. Also, because of the relatively high pressure in the vicinity of the slit, a significant amount of charge exchange takes place, thus creating a component of high energy molecules. By deflecting the ion beam out of the mainstream of the background gas and the energetic molecules, the effect of these two components on the target force is negligible. Figure 2 shows that the back and sides of the turning stage are open so that these two components may escape.

The narrow rectangular form was chosen for the ion beam because it is easier to contain and to deflect electrostatically than a circular beam with the same cross-sectional area. The beam was extracted from the main anode region through a thin slit accelerator plate with dimensions of 1.3 × 0.008 cm. The subsequent path of the ions is best shown in the schematic diagram of Fig. 3. The ions were extracted from the main anode region at 300 to 400 eV energy. They were then electrostatically turned, collimated, and decelerated before striking the target. Target currents ranged from about 3 μA at 9 eV ion energy up to 10 μA at 30 eV and above. Ideally, the potential difference between the axisymmetric turning-stage elements should be constant along the path, but geometric and space-charge effects complicate the problem. Therefore, the inner element of the turning stage was segmented so that this stage could be tuned to give a maximum transmission of ions and to properly align the ion beam with the target.

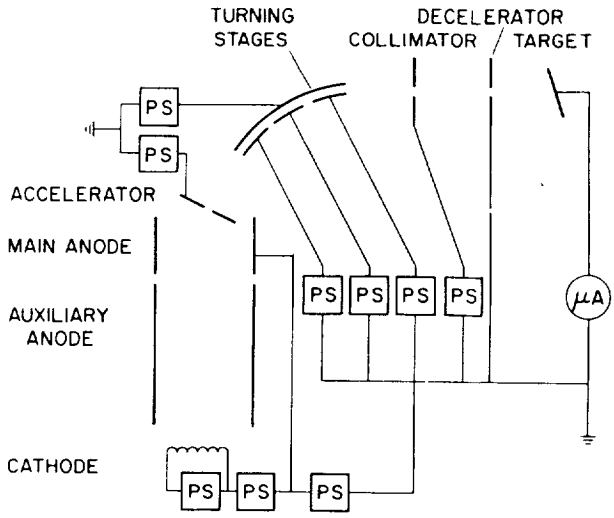

FIG. 3. Electrical schematic of system.

The vacuum was maintained in the test chamber with two 6-inch oil diffusion pumps operating in parallel. The pumps were charged with Dow-Corning 705 Silicone Pump Oil. Backstreaming oil was inhibited by standard baffle traps loaded with oil-absorbing zeolite. The effectiveness of the traps was improved by adding refrigeration lines from a Freon-12 system to the baffles of the standard trap. As a further precaution diffusion pump oil was used in the fore pumps to minimize backstreaming from that source. To check the effectiveness of the trap, a thin quartz plate was left in the entrance to the angle valve (Fig. 1) during a week of continuous pump operation.

This plate was then checked for evidence of oil deposits on an ultraviolet absorption spectrophotometer which was sensitive to oil deposits down to 1-monolayer thick, [11] but no oil was detected.

For typical operation, the system was pumped down to the low 10^{-7} torr range and maintained at that pressure for several hours. The system was then backfilled with N_2 gas to an operating pressure in the high 10^{-6} torr range for the test chamber and the discharge was started. The discharge was then allowed to run several hours before taking data so that thermal equilibrium could be reached and the ion gun assembly outgassed.

The vacuum microbalance used in this experiment was a modification of a standard Rodder Instrument microbalance. [9, 12] The deflecting element of the balance is the long horizontal quartz fiber shown in Fig. 1. The balance is operated as a nulling instrument. The null is set by manually turning the quartz fiber, and the null is detected with a photocell system. The overall sensitivity of the system is 0.05 mdyn. The target and a counterbalance hang vertically from the two ends of the balance crossarm so the balance can measure only vertical forces. For the ion gun position of Fig. 1, the ion beam is horizontal when it reaches the target so that the lift force on the target is measured. To measure the drag force the ion-gun assembly is mounted on the wall opposite the manipulator shafts with the ion beam directed vertically upward.

To measure current to the target a tungsten wire 15 cm long and 4×10^{-4} cm in diameter was connected to the suspension crossarm on which the targets were hung. This crossarm was fitted with a thin-walled platinum sleeve to make electrical contact with the target hook. The wire lead was loosely suspended from the balance to minimize interference with the balance readings. The fact that the balance was operated as a null instrument with minimal deflections also minimized the possibility of interference. To check that there was no interference, several wire samples were weighed with and without the lead wire in place. No difference in weight was observed. As a final precaution, the balance was calibrated with the wire in place.

The targets were made of commercial-grade sheet aluminum and prior to being tested were cleaned with chemically pure acetone in a sonic bath. No effort was made to have the targets atomically clean, because at the background test pressure of 10^{-5} torr a monolayer of gas would be deposited in less than a second. The tests were then made on target surfaces which were reasonably clean but covered with atmospheric gas. This is also the probable condition of many earth satellite surfaces because calculations show that at altitudes up to 200 km the gas flux swept up by the satellite surface, because of its velocity, is comparable to the thermal flux to the targets at 10^{-5} torr pressure.

The targets were soldered to stainless steel tubing with carefully made hooks at the top (Fig. 1) so that the targets would hang freely from the suspension crossarm. Each target was soldered to its stem so that it would have a fixed angle of incidence to the ion beam when hanging from the balance. Target incidence angles measured from the normal to the surface ranged from 0° to 75° in 15° increments. A storage rack was provided inside the test chamber so that these targets could be interchanged while the system was operating

Experimental Procedure and Data Reduction

The total force on the target consists of two parts—the incident force caused by impact of the beam particles and that caused by their subsequent reflection. This is also true of each vector component of the total force, whether taken as lift and drag or as forces normal and tangential to the surface. To obtain the momentum accommodation coefficients requires determining both the incident and reflected parts of normal and tangential forces. For the present tests, these, in turn, had to be determined indirectly from the measured total lift and drag forces together with the measured ion energy spectrum and the ion current to the target. From the latter two measured quantities the incident forces may be calculated.

Of these quantities, the lift and drag forces were the most difficult to measure. Even though the ion beam was deflected out of the main stream of gas streaming from the anode, a small fraction of nonionized gas followed through the turning stage and contributed a small tare force on the targets. This constant tare force on the target together with any thermal drift of the microbalance readings was accounted for by using as a continuing reference the corresponding microbalance readings taken with the ion beam off. At least five individual pairs of data were recorded and averaged for each data point.

The ion current to the target was measured simultaneously with each force measurement. The primary concern with this measurement was that secondary electrons emitted from the surface might give a spuriously high ion current reading. This effect was found to be negligible when checked using a probe designed to collect electrons near the target under operating conditions. The energy distribution of the ion beam was measured with a flat-plate retarding-potential probe. This was done prior to

each data run and occasionally after a run to check the steadiness of the energy distribution.

Data were taken in the preceding fashion for a matrix of nominal ion energies between 9 and 40 eV and of beam incidence angles between 0° and 75°. This matrix was repeated for both the lift measurements and the drag measurements. Repeat data were taken to determine the reliability of the data.

The raw data were first reduced to the ratios L/I and D/I, where L and D are measured lift and drag and I is the current to the target at the time the balance was nulled. The next step was to reduce the L/I and D/I data to the traditional tangential and normal momentum accommodation coefficients

$$\sigma' = (p_i - p_r)/(p_i - p_s) \tag{1}$$

$$\sigma = (\tau_i - \tau_r)/\tau_i \tag{2}$$

where τ and p denote tangential and normal momentum flux, respectively, and the subscripts i and r denote incident and reflected components, respectively. The term p_s is the normal momentum flux of the gas if it were reflected diffusely at the surface temperature. Using the geometric relations of L and D to the normal and tangential components, then for a monoenergetic beam of ions, Eqs. (1) and (2) become:

$$\sigma' = \{2 - (e/mv_i)[(D/I) + (L/I)\tan\theta_i]\}/[1 - (p_s/p_i)] \tag{3}$$

$$\sigma = (e/mv_i)[(D/I) - (L/I)\cot\theta_i] \tag{4}$$

where e is the unit electric charge, m is the mass, v_i is the speed of the incident ion, and θ_i is the incidence angle to the normal. The method of Schamberg [13] indicates that:

$$p_s/p_i = (\tfrac{2}{3})(v_s/v_i\cos\theta_i) \tag{5}$$

where $v_s = (8kT/\pi m)^{1/2}$ is the mean thermal speed of the gas molecule at the temperature of the surface. For the nitrogen molecule, Eqs. (3) and (4) become:

$$\sigma' = 2 - [13.10/\sqrt{(E)}]\,[(D/I) + (L/I)\tan\theta_i]/ \times [1 - (0.0070/\cos\theta_i)\sqrt{(T/E)}] \tag{6}$$

$$\sigma = [13.10/\sqrt{(E)}]\,[(D/I) - L/I)\cot\theta_i] \tag{7}$$

where E is in eV, D and L in mdyn, I in μA, and T in °K. For these equations it was assumed that the surface temperature was the same for both the lift and the drag measurements, as was sufficiently true for the present test. Eqs. (6) and (7) were derived on the assumption of a monoenergetic beam of ions. However, for this experiment the energy spectrum was sufficiently broad that a more elaborate procedure was devised to ensure obtaining accurate values of σ and σ' from the data. In this procedure, Eqs. (6) and (7) were used to establish approximate values for σ and σ' from which perturbations were made to determine more precise values.

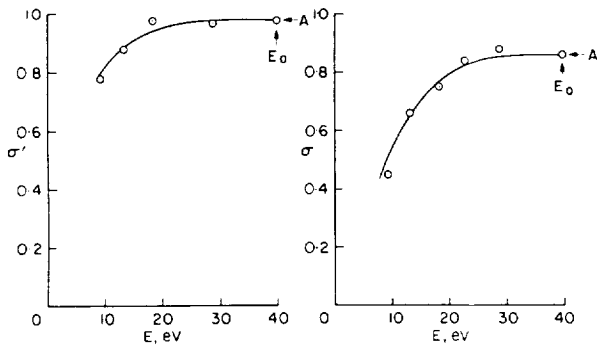

FIG. 4. Typical fitting to preliminary data of functions σ (or σ') $= A - B(E_0 - E)^N$; (a) normal, (b) tangential.

In Fig. 4, typical approximate data of this type show the variations of σ and σ' with E. The data points on these curves were calculated from Eqs. (6) and (7) using experimental values for L/I and D/I, and an effective value for E. This effective energy is the so-called half-max value obtained from probe curves typified in Fig. 5, which shows the variation of ion current with retarding potential for a flat-plate probe normal to the ion beam. The half-max energy is the retarding potential at which the current is reduced to one-half its unretarded value.

The curves that approximate the data points in Fig. 4 are calculated from equations of the form

$$\sigma(\text{or } \sigma') = A - B(E_0 - E)^N \tag{8}$$

where A, B, E_0 and N are curve fitting constants. These constants were calculated using a program to give the least-squares fit to the data. It was found that for all angles of incidence the data could be well approximated by this functional form. The accuracy of fit shown in Fig. 4 is typical of the fit for all data presented herein.

The energy spectrum showing the degree to which the ion beam deviates from a monoenergetic beam is shown in Fig. 6. The ordinate dI/dE was obtained from probe data like that shown in Fig. 5. This was done by a curve fairing and differentiation procedure that was programmed on a digital computer. In all cases, the half-max energy was less than the energy at maximum dI/dE by 1 to 2 eV.

With this information an iterative procedure was formed for a more accurate determination of σ and σ'

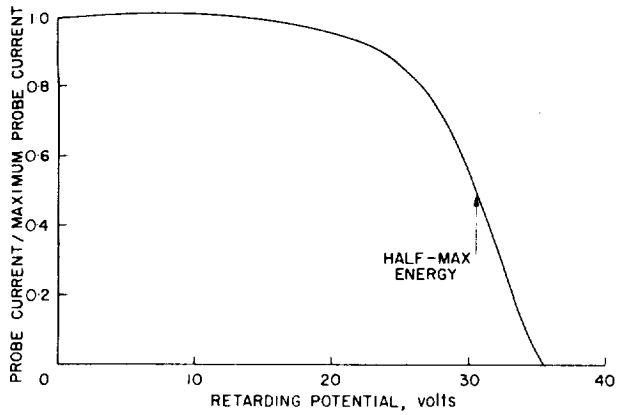

FIG. 5. Characteristic curve for retarding potential probe.

from the data. Eqs (6) and (7) were inverted and written in differential form

$$dL = (\sin\theta_i \cos\theta_i/13.10)\{2 - \sigma'(E) \times [1 - (0.0070/\cos\theta_i)\sqrt{(T/E)}] - \sigma(E)\} \times \sqrt{(E)}(dI/dE)dE \quad (9)$$

$$dD = (\cos^2\theta_i/13.10)\{2 - \sigma'(E)[1 - (0.0070/\cos\theta_i) \times \sqrt{(T/E)}] + \sigma(E)\tan^2\theta_i\}\sqrt{(E)}(dI/dE)dE \quad (10)$$

The quantity dI/dE was known experimentally from the probe data for each of the six nominal values of energy for which L/I and D/I were measured. The functional form of $\sigma(E)$ and $\sigma'(E)$ was known (Eq. (8)), but the values of the eight constants (four for σ and four for σ') were known only approximately. The iterative procedure operated on these constants until the quantity

$$\sum[(L/I)_{ex} - (L/I)_{in}]^2 + \sum[(D/I)_{ex} - (D/I)_{in}]^2 \quad (11)$$

was minimized. Here the subscript ex refers to an experimental value for one of the nominal energies and the subscript in refers to the integrated value

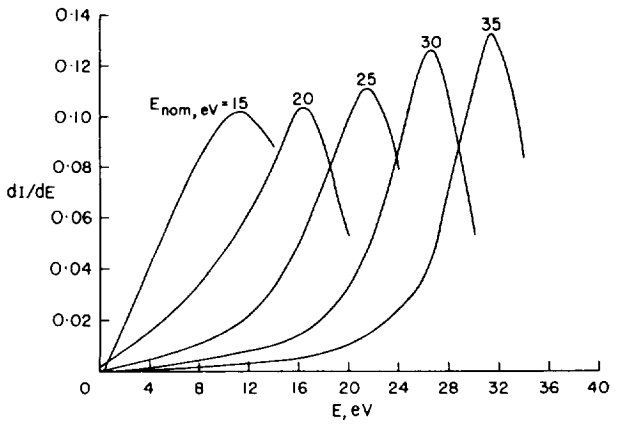

FIG. 6. Energy distributions of ion beam.

using either Eq. (9) or (10) and the dI/dE data for the same energy.

The final values of σ and σ' calculated by this procedure never differed from the approximate value calculated from Eqs. (6) and (7), by more than the experimental spread in the data, provided that the half-max value was used for the effective value of E. However, if other values were used for E, such as those corresponding to peak values of dI/dE (Fig. 6), the difference was generally larger than the experimental spread, particularly for the smaller values of E.

Analysis

Relation between momentum transfer for N_2 and N_2^+. Molecular nitrogen is the primary contributor to the momentum transfer between a satellite and the atmosphere up to an altitude of about 300 km. An experiment using one gas species to study the forces and moments on a satellite, therefore, should use molecular nitrogen. However, it is difficult to obtain a beam of molecular nitrogen in the satellite speed range with sufficient flux and with sufficiently well-defined energy characteristics to make accurate measurements. These requirements are more easily met if a beam of diatomic nitrogen ions is used. The problem then remains to relate the measurements with N_2^+ to those one would obtain with N_2.

Fortunately the difference between using N_2 or N_2^+ as the impacting particle for momentum transfer measurements is not large. Experimental evidence shows that essentially 100 per cent of the ions approaching a surface are neutralized prior to striking the surface. In effect, this constitutes a charge-exchange system which is much more efficient than passing the ion beam through a conventional charge-exchange chamber.

Several mechanisms are possible for ion neutralization at a surface, but for the ion energy range of this investigation, neutralization is accomplished by Auger transition. [14, 15] In this process a free electron is ejected from the metal surface to neutralize the approaching ion. The energy lost by this neutralizing electron is, in the case of monoatomic particles, transferred to a second electron that may have sufficient energy to escape and become a free secondary electron. However, Prince [14] has shown that for diatomic particles some of this excess energy is absorbed by the neutralized ion and its vibrational mode is excited. Thus, the probability for secondary electron emission by diatomic molecules is much less than for atoms. This at least partially explains the observed fact mentioned earlier that secondary

electrons were not observed in the vicinity of the targets.

Although ions are neutralized before striking a metal surface, there are still some differences between ion and molecular interactions with a surface that must be considered. Because of imaging effects, an ion is accelerated toward the surface more than a neutral molecule prior to the neutralization process, and strikes the surface with more momentum. If the momentum of this particle is fully accommodated by the surface there is no net change of momentum due to this effect, because the target also acquires a momentum component of equal magnitude but opposite direction and these two components are exactly cancelled on impact. However, if the particle momentum is not fully accommodated, the additional energy acquired on the approach must be considered. Prince[14] and Mair, Viney, and Colligan[7] show that this incremental energy is approximately

$$\Delta E = 3.6/S_0 \qquad (12)$$

where ΔE is in eV and S_0 is the distance in Å between the surface and the ion when Auger transition takes place. This average distance is about 4 or 5 Å so that ΔE is about 1 eV or less. In appendix A it is shown that the differences in accommodation coefficients due to using ions rather than neutral nitrogen molecules as the test particle are small compared to the repeatability of the present data and therefore can be neglected.

Collision Model. It is not reasonable to construct an elaborate theory for comparison with the present data because the detailed nature of the surfaces used is not known. However, it is helpful for understanding the data to have some form of model in mind. For this purpose a simple physical model is postulated and the results of some calculations using this model will be used in the discussion of the data to explain the trends observed. The model is a simplified version of the one used by Jackson [16] which, in turn, is a simplification of the model used by Oman. [17] The basis for these models is well discussed in the literature. [3, 16, 17] Therefore, only comments necessary for the present treatment will be made. These models are all constructed for neutral incident particles rather than ions, but in view of the discussion in the previous section, the qualitative trends should be the same.

As an atom approaches a solid surface it interacts with the potentials of many surface atoms simultaneously, and an exact solution to the problem becomes extremely complex. To simplify the calculation, Jackson [16] approximated the physical surface with hard spheres to provide the repulsive part of the potential field and a one-dimensional attractive field over the surface to represent the integrated attraction of all surface atoms. He also neglected any coupling between atoms in the surface on the rationalization that the reaction time between lattice atoms is much larger than the reaction time between gas and surface atoms for gas atoms with satellite velocity. With this model, Jackson was able to obtain reasonable agreement with the calculated results of Oman who uses a more elaborate model. All of these assumptions are incorporated in the present analysis.

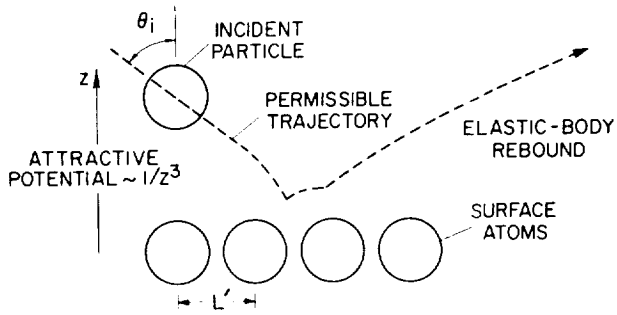

FIG. 7. Cross section of trajectory for theoretical model.

A sketch of the physical model used is shown in Fig. 7. The repulsive portion of the surface potential is simulated by hard spheres uniformly spaced L' Å apart. The radius of these spheres depends on the surface atoms, the gas, and the energy of the incident gas particle. The effective radius is inversely related to the energy because the high energy particles can penetrate further into the repulsive potential. The attractive portion of the surface potential is averaged over all surface atoms and seems to be best approximated by an inverse cubic form [18]. One of the

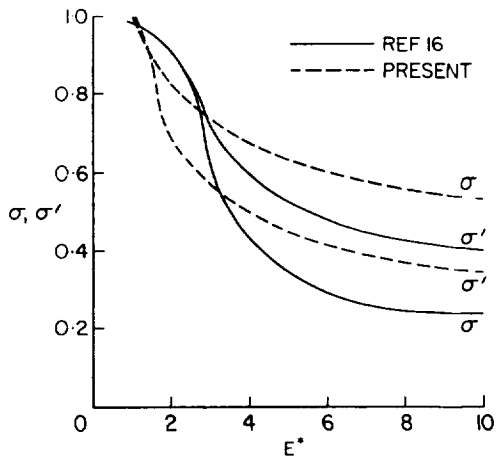

FIG. 8. Comparison of theories for energy variation, $\theta_i = 45°$, $R/L' = 1.3, \mu = 0.217$.

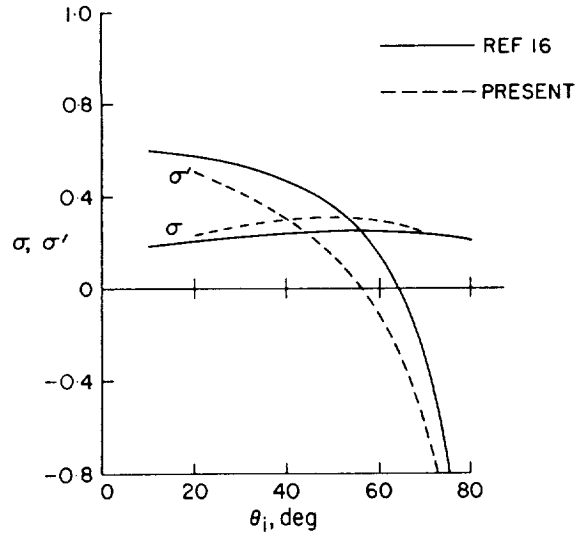

FIG. 9. Comparison of theories for angle of incidence variation: $E^* = 9.5, R/L = 1.3, \mu = 0.217$.

possible particle paths is shown in the sketch, but many others are possible. These range from collision with one surface atom to multiple collisions and ultimate capture of the particle. To determine momentum accommodation coefficients from this model, a number of particles are directed toward the surface, all at a fixed angle of incidence, θ_i, and the average momentum change due to the interactions with this model is calculated.

Results of some calculations of σ and σ' using the present method are compared with those of Jackson [16] in Figs. 8 through 11. Comparisons are made of the trends with all four parameters, E^*, μ, R/L, and θ_i,

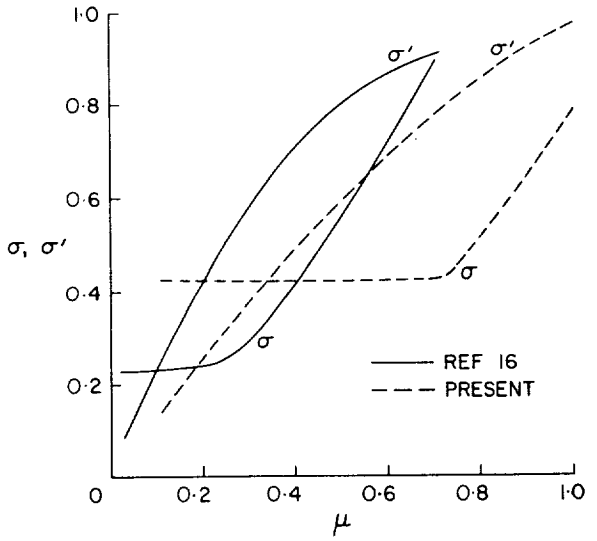

FIG. 10. Comparison of theories for mass ratio variation: $E^* = 9.5, \theta_i = 45°, R/L = 1.3$.

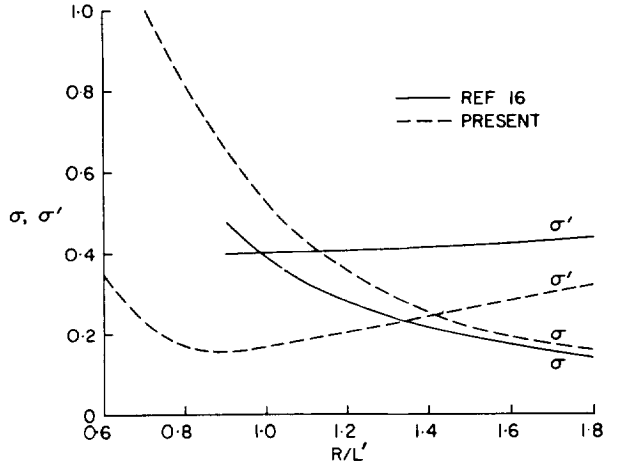

FIG. 11. Comparison of theories for lattice spacing variation: $E^* = 9.5, \mu = 0.217, \theta_i = 45°$.

on which σ and σ' depend. The ratio of the impinging particle energy to the energy of the attractive field of the surface is E^*; the ratio of the mass of the particle to the mass of the surface atom is μ; and the distance between centers of the particle and the surface atom at impact is R. In general, the magnitudes given by the two methods do not agree, but the qualitative trends are similar. On the basis of this qualitative agreement the use of calculations by the present simplified method to explain trends in data appears justified.

It is of interest that the foregoing trends of σ' were the same for a two-dimensional version of the present model, but that those trends of σ were not generally the same. The implication is that, at least for the range of variables presently considered, the normal momentum exchange is more simply described than is the tangential momentum exchange. This might be expected *a priori* because for each gas particle the reflected normal momentum component is in the same plane as the incident momentum and a surface normal, but the reflected tangential momentum component can be in any of an infinite number of planes.

Results and Discussion

Experimental results. The results of the present experimental investigation are summarized in Fig. 12. The normal and tangential momentum accommodation coefficients are presented as functions of ion energy for a series of incidence angles. The data are shown as curves rather than points because the integration process described in the data reduction section loses the identity of energy with a given measurement. Where several sets of data were taken

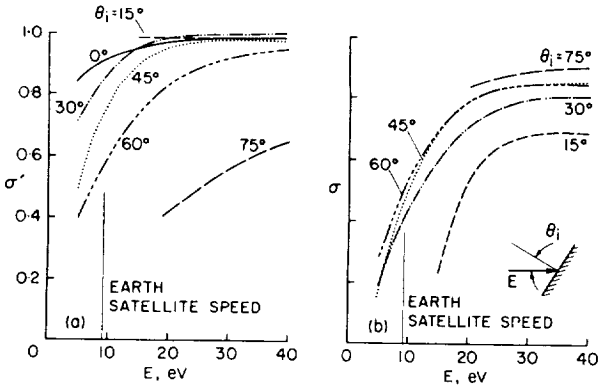

FIG. 12. Variations of momentum-accommodation coefficients with ion energy for N_2^+ on aluminum: (a) normal, (b) tangential.

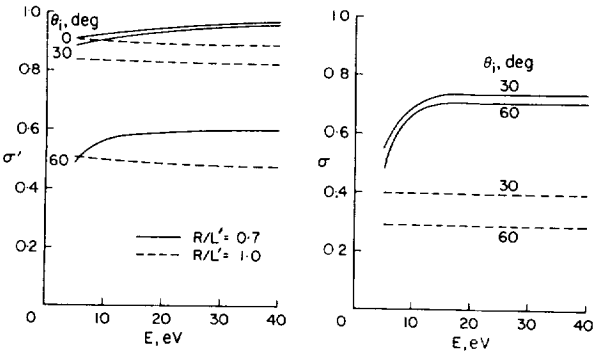

FIG. 13. Calculated variations of σ and σ' with energy, $\mu = 0.9$: (a) normal, (b) tangential.

for a given angle, the curves in Fig. 12 represent the average values. On the basis of repeatability of data, the maximum uncertainty in σ or σ' for those curves is ± 0.05 except for the $\theta_i = 75°$ and 15° curves for parts (a) and (b), respectively. For these curves the uncertainty is ± 0.1 for the highest energy and ± 0.15 for the lowest energy. The large uncertainties for these angles are a consequence of the fact that only a small component of the total force on the target is measured; hence, the magnitude of the forces measured is much smaller than for the other angles.

The major trend exhibited in Fig. 12 is the decrease in both normal and tangential momentum accommodation with decreasing energy, σ and σ' varying from as high as 1.0 at $E = 40$ down to about 0.2 for σ and 0.4 for σ' at the lower energies. Such a trend in σ' has been observed in this energy range by other investigators [5, 7] but the opposite trend has been observed as well [19]. Nitrogen was used in all four of these investigations (including the present one) and Al surfaces were used in all of them except that of Ref. 7 where Cu was used. Earlier results by the present investigators also found a decrease in the accommodation coefficients with decreasing energy for argon ions on aluminium [9]. Therefore, this trend with energy is possible for both monatomic and diatomic incident particles.

Calculations using the model described in the Analysis section show in Fig. 13 that different trends with energy are possible, depending on the ratio R/L. Although, as expected, the magnitudes do not compare well with the data of Fig. 12, the trends exhibited by the set of solid curves for $R/L = 0.7$ are quite consistent with the data, whereas the trends exhibited by the set of dashed curves for $R/L = 1$ are not consistent with the data. For a perfect crystal surface, values a little larger than 1 for R/L would be expected. However, for unclean engineering surfaces with lattice vacancies, steps, and scratches, the effective lattice spacing L would be expected to be larger, and values of R/L less than 1 are possible. No attempt was made to determine the actual value of R/L for the conditions of this experiment, but it is clear that the character of target surfaces must be known if reliable comparisons are to be made with theory.

The model shown in Fig. 7 offers a physical explanation for the variations with energy shown in Fig. 13. It relates to the fact that the effective radii of the surface spheres diminish with increasing energy. It is apparent from Fig. 7 that the maximum depth to which an incident particle can penetrate between surface atoms is greatest for small particles, i.e., for small values of R/L. (If $R/L < 0.5$, some particles could pass completely through the outer surface layer.) Usually the momentum accommodation of a particle increases with the depth of penetration. Because R is effectively less for the higher energy particles than for the lower energy particles, it follows that there is a tendency for deeper penetration, hence, increased momentum accommodation as the energy is increased. Calculations show that this effect is most pronounced for small values of R/L (see dashed curves of Fig. 11). For values of R/L of the order of 1 and greater, other

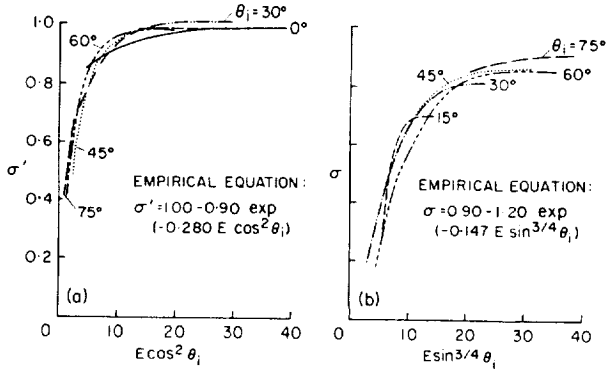

FIG. 14. Correlation of momentum-accommodation data: (a) normal, (b) tangential.

effects become important and the trend with energy is reversed for σ'.

An interesting correlation is shown in Fig. 14 for the data of Fig. 12. Figure 14(a) shows that the σ' data for all values of θ_i are correlated to within the precision of the data by the parameter $E\cos^2\theta_i$. This correlation suggests that, at least for the conditions of this experiment, the normal momentum behaves as if it were uncoupled from the tangential momentum. If these two components of momentum were actually uncoupled, the tangential momentum accommodation coefficient, σ, should be correlated by the corresponding parameter $E\sin^2\theta_i$. It is not, but instead, is more nearly correlated by the parameter $E\sin^{3/4}\theta_i$, as shown in Fig. 14(b). This difference in the variations of the normal and tangential components is consistent with the discussion in the Analysis section where it was noted that σ' is qualitatively described by a two-dimensional model, but that σ requires the more complex three-dimensional model. The coefficient σ', therefore, appears to be more simply related to the governing parameters than is σ.

The value of these correlation parameters is that they facilitate the integration procedures necessary to calculate forces and moments on satellites of arbitrary shape. In particular, they provide a means of extrapolating to large angles of incidence (near grazing angle) for which it is difficult to obtain experimental data.

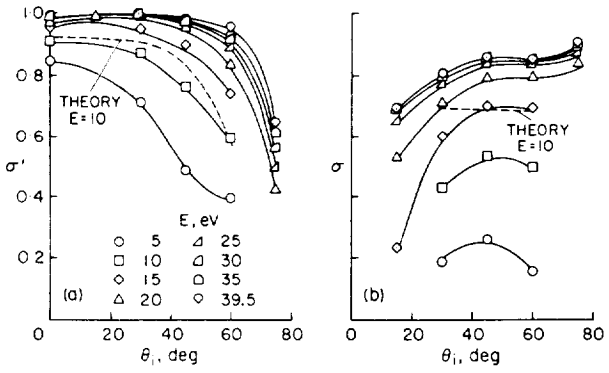

FIG. 15. Variations of momentum-accommodation coefficients with incidence angle for N_2^+ on aluminum: (a) normal momentum, (b) tangential momentum.

In Fig. 15 the experimental values of σ and σ' are shown as functions of incidence angle for various energies. The most striking trend apparent in these data is the sharp decrease in σ' at the larger, or more glancing, incidence angles. This trend has previously been observed [9] for argon ions incident on both aluminum and gold surfaces and in fact was a postulation leading to both the investigation of Ref. 9 and the present tests. Tangential momentum showed a generally opposite trend, however, with σ tending to decrease at the smaller incidence angles.

The dashed curves (crossplots from Fig. 13) show the calculated variations of σ' and σ with θ_i for an energy of 10 eV. Comparison of these curves with the experimental results shows that the variation of σ' with θ_i is qualitatively well predicted. However, the calculated values of σ vary much less with θ_i than do the experimental values.

A trend with θ_i that is more consistent with the data can be calculated using the present model if a mass ratio less than 0.2 is used. Although the mass ratio for the experimental system is not known, it is not likely to be as low as 0.2 and is more likely to be of the order of unity. Again it appears that the tangential component of momentum is more difficult to analyze than is the normal component, and that a good knowledge of the physical parameters of the surface is necessary for a complete analysis of experimental data of this type.

Applications. The momentum accommodation coefficients were historically defined for free-molecule flow conditions; it is to this flow regime that the present paper is directed. In particular, the motivation for the program reported here was to improve the understanding of the forces and moments acting on earth satellites. However, it may be mentioned in passing that it has become increasingly apparent that knowledge of accommodation coefficients is also important for the understanding of gas-surface boundary problems in the transition and slip flow regimes [1]. The slip coefficient and the onset of continuum-flow behavior can be significantly influenced by the degree of accommodation [20]. Knowledge of momentum accommodation coefficients is, therefore, also necessary for an accurate analysis of the aerodynamics of high flying aircraft and of vehicles beginning to enter an atmosphere.

Perhaps the most important application of momentum accommodation coefficients to satellites concerns the torques on the vehicle due to interaction with gas. This gas can be either the atmospheric gas or gas from leakage or exhaust of attitude control units. The impingement of these latter sources of gas on the vehicle can create significant problems regarding attitude and trajectory control and the fuel requirements to correct them. For the analysis of these torques the assumption is frequently made that momentum is fully accommodated at the surface. That this is not an adequate assumption is demonstrated in Fig. 16. In this figure the torque on a flat-plate element with momentum accommodation

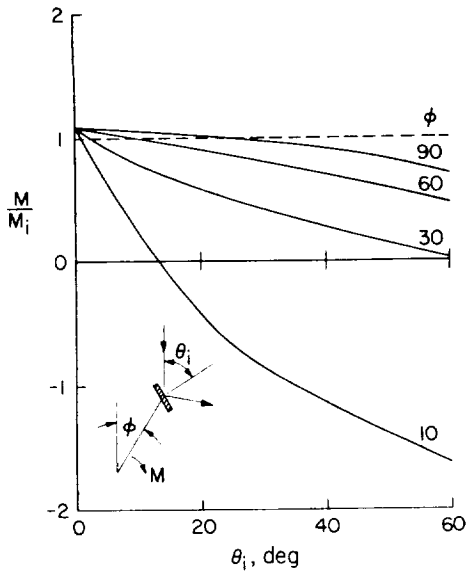

FIG. 16. Effect of incomplete momentum accommodation on the torque of a surface element.

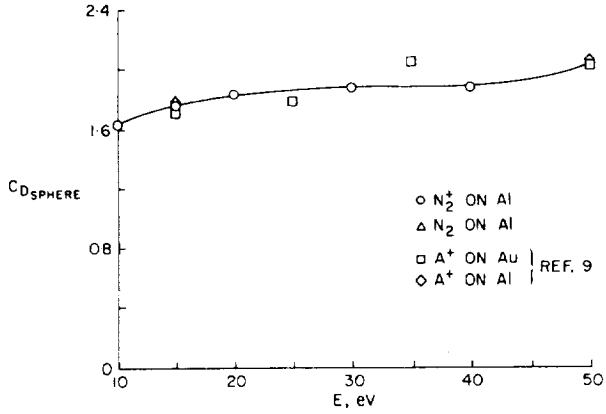

FIG. 17. Sphere drag coefficients for experimental σ, σ'.

according to the present results is related to the torque for full accommodation for $E = 9$ eV which is the energy of N_2 at near-earth satellite velocity. These data are plotted against θ_i for four values of the azimuth angle ϕ defined by the sketch in the figure. For $\phi = 90°$, the drag forces measured in this investigation could have been converted directly to torque without the necessity of measuring two components of force. However, for general values of ϕ it is necessary to have measured both normal and tangential components. The figure shows that the deviation from full accommodation values can be considerable.

As noted previously, these experiments were begun partly because of a postulation that the accommodation coefficients could vary with θ_i in such a manner as to permit values of drag coefficient less than 2 for a spherical satellite. For this reason it will be informative to use the experimental values of σ and σ' to make such a calculation. When the drag components of normal and tangential forces are integrated over the forward surface of the sphere and made dimensionless in the usual form, the resulting equation takes the form,

$$C_{D,\,\text{sphere}} = 4 \int_{\theta_i = 0}^{\pi/2} [\sigma \sin\theta_i \cos\theta_i + (2 - \sigma - \sigma') \sin\theta_i \cos^3\theta_i] d\theta_i \qquad (13)$$

When the experimental values of σ and σ' were used to evaluate this equation, the resulting values of sphere drag coefficient are as shown in Fig. 17. Note that all values for the present tests are less than 2.0 and that generally similar results are found using the data of Ref. 9 for argon on both aluminum and gold surfaces. One value of drag coefficient has also been calculated from the present results after correcting them to the equivalent molecular impact, and this value shows a negligible effect of such a correction. From the results of Fig. 17, one may speculate that drag coefficients for spherical satellites may be somewhat less than those generally used, which are about 2.2.

Conclusions

The tangential and normal momentum accommodation coefficients have been measured for N_2^+ impinging on aluminum surfaces at speeds ranging from slightly below to about twice earth-satellite speed. The following conclusions are drawn from an analysis of these data.

1. Even for surfaces that are not atomically clean, the accommodation of normal and tangential momentum can be far from complete.
2. Both components are strongly dependent on the incident particle energy. The accommodation of both components decreases rapidly with energy in the range of interest for earth satellites.
3. The accommodation of the normal component of momentum decreases rapidly as the incidence angle approaches the grazing value. Conversely, the accommodation of the tangential momentum increases, but the effect of incident angle on the tangential component is generally less than for the normal component.
4. The normal momentum-accommodation coefficient data from this investigation are correlated by the parameter $E \cos^2\theta_i$ and the tangential momentum-accommodation coefficient by the parameter $E \sin^{3/4}\theta_i$.

5. A simple classical model can be used to explain many of the trends exhibited by the data. The normal component of momentum appears to be easier to model than is the tangential component.
6. The torque on a satellite element due to impingement of atmospheric gas or reaction control gas can differ considerably from that to be expected if momentum were completely accommodated.
7. The drag coefficient for a spherical satellite can be considerably less than the 2.2 value commonly used.
8. It is shown that the results presented here for the N_2^+ ion on aluminum are only slightly different from those to be expected for the N_2 molecule on aluminum.

References

1. PATTERSON, G. N., A state-of-the-art survey of some aspects of the mechanics of rarefied gases and plasmas, USAF Report ARL 64–60 (1964).
2. SCHAAF, S. A. Aerodynamics of satellites, RAND Corp. Report R–339, 1-1–1-14 (1959).
3. HURLBUT, F. C., Current developments in the study of gas-surface interactions, Univ. of Calif. Engineering Report AS–66–10 (1966).
4. FAN, C. and WARR, J. W., Gas-surface interactions and orbital aerodynamic calculations, Lockheed Report HREC D 162–228 (1970).
5. BORING, J. W. and HUMPHRIS, R. R., Drag coefficients for free-molecule flow in the velocity range 7–37 km/sec, *AIAA J.*, **8**: **9**, 1558–1662 (1970).
6. ABUAF, N. and MARSDEN, D. G. H., Momentum accommodation of argon in the 0.06 to 5 eV range, *Rarefied Gas Dynamics*, Supplement **4**, **1**, 199–210 (1967).
7. MAIR, W. N., VINEY, B. W., and COLLIGON, J. S., Experiments on the accommodation of normal momentum, *Rarefied Gas Dynamics*, Supplement **4**, **1**, 187–198 (1967).
8. OMAN, R. A. and CALIA, V. S., Gas-surface interaction research, Grumman Report RE–365 (1969).
9. KNECHTEL, E. D. and PITTS. W. C., Experimental momentum accommodation on metal surfaces of ions near and above earth-satellite speeds, *Rarefied Gas Dynamics*, Supplement **5**, **2**, 1257–1266 (1969).
10. PITTS, W. C. and KNECHTEL, E. D., Experimental investigation of electric drag on spherical satellite models, NASA TN D–2619 (1965).
11. SUPPLE, R. W. and GLORIA, H. R., Spectrophotometer for continuous measurement in vacuum systems of polyphenyl diffusion pump fluid film thickness, *J. Vacuum Sci. and Tech.* **4**: **5**, 276–278 (1967).
12. PLANT, A. F., A little weight, *Industrial Res.* **13**: 7, 36–39 (1971).
13. SCHAMBERG, R., A new analytic representation of surface interaction for hyperthermal free molecule flow with application to neutral-particle drag estimates of satellites, RAND Corp. Report RM–2313 (1959).
14. PRINCE, R. H., Interaction of low-energy atmospheric ions with controlled surfaces, University of Toronto, UTIAS Report 133 (1968).
15. KAMINSKY, M., *Atomic and Ionic Impact Phenomena on Metal Surfaces*, 263–268, Academic Press (1965).
16. JACKSON, D. P., A theory of gas-surface interaction at satellite velocities, University of Toronto, UTIAS Report 134 (1968).
17. OMAN, R. A., Research in gas surface interactions, Part I. Numerical calculations of gas surface interactions, Grumman Research Report RE–222 (1965).
18. BOWDEN, F. P., *The Nature and Topography of Solid Surfaces and the Study of Van der Waals Forces in Their Immediate Vicinity*, Fundamentals of gas surface interactions, 1–24, Academic Press (1967).
19. DOUGHTY, R. O. and SCHAETZLE, W. J., Experimental determination of momentum accommodation coefficients at velocities up to and exceeding earth escape velocity, *Rarefied Gas Dynamics*, Supplement **5**, **2**, 1035–1054 (1969).
20. EPSTEIN, M., Effect of incomplete accommodation on the slip coefficient, Aerospace Corp. Technical Report TR–0158(3240–20)–12 (1968).

Appendix A

Effect of using ions rather than molecular nitrogen. For the purpose of measuring the momentum accommodation coefficients, the primary difference between using ions or the corresponding molecules will be in the final energy of the particle as it strikes the surface. It was stated in the text that this energy difference, ΔE, is of the order of 1 eV or less. For values of E that are large relative to ΔE the difference between using ions or neutral molecules is small, but this is not necessarily the case for small values of E. An estimate of the differences to be expected will, therefore, be made in this appendix.

The defining Eq. (1) includes the effect of surface temperature, but this effect alters σ' by only a few per cent at most and can be ignored for the present estimation. Eqs. (1) and (2) can then be written as

$$\sigma(E) = 1 - (\tau_r/\tau_i), \text{ or}$$

$$\sigma(E) = 1 - [(D_r \sin\theta_i - L_r \cos\theta_i)/\lambda I\sqrt{(E)} \sin\theta_i] \quad \text{(A1)}$$

and

$$\sigma'(E) = 1 - (p_r/p_i), \text{ or}$$

$$\sigma'(E) = 1 - [(D_r \cos\theta_i + L_r \sin\theta_i)/\lambda I\sqrt{(E)} \cos\theta_i] \quad \text{(A2)}$$

Here the denominators are the values of τ_i and p_i calculated from the measured values of target current and average ion energy, and λ is a proportionality factor. The terms D_r and L_r are the components of drag and lift caused by rebound of the impacting particles. Consider Eq. (A2) and let $D_r = D_+$ and $L_r = L_+$ for the ion case and $D_r = D_m$ and $L_r = L_m$ for the molecular case. Then Eq. (A2) becomes:
For molecules,

$$\sigma'_m(E) = 1 - \{[D_m(E) + L_m(E) \tan\theta_i]/\lambda I\sqrt{(E)}\} \quad \text{(A3)}$$

and for ions,

$$\sigma'_+(E) = 1 - \{[D_+(E) + L_+(E)\tan\theta_i]/\lambda I\sqrt{(E)}\} \quad \text{(A4)}$$

Now D_+ and L_+ differ from D_m and L_m primarily because the ions strike the surface with a greater energy than the molecules. If the molecules were given a larger initial kinetic energy, $E + \Delta E$, equal to the ion energy after acceleration to the surface, the reflection characteristics for the ions and molecules should be similar. Then we would have very nearly

$$D_+(E) = D_m(E + \Delta E) \quad \text{(A5)}$$

and

$$L_+(E) = L_m(E + \Delta E) \quad \text{(A6)}$$

From Eq. (A3)

$$\sigma'_m(E + \Delta E) = 1 - \{[D_m(E + \Delta E) + L_m(E + \Delta E)\tan\theta_i]/\lambda I\sqrt{(E + \Delta E)}\} \quad \text{(A7)}$$

which becomes, using Eqs. (A5) and (A6)

$$\sigma'_m(E + \Delta E) = 1 - \{[D_+(E) + L_+(E)\tan\theta_i]/\lambda I\sqrt{(E)}\}\sqrt{[E/(E + \Delta E)]} \quad \text{(A8)}$$

Upon substitution from (A4), we have

$$\sigma'_m(E + \Delta E) = 1 - [1 - \sigma'_+(E)]\sqrt{[E/(E + \Delta E)]} \quad \text{(A9)}$$

Similarly for the tangential momentum accommodation coefficient,

$$\sigma_m(E + \Delta E) = 1 - [1 - \sigma_+(E)]\sqrt{[E/(E + \Delta E)]} \quad \text{(A10)}$$

These last two equations then relate the accommodation coefficients measured for ions at energy E to the corresponding accommodation coefficients for the molecules at a slightly larger energy, $E + \Delta E$. These equations show that if either the accommodation coefficient approaches unity or ΔE approaches zero, the differences between the ion and molecular values for σ or σ' approaches zero.

The largest magnitude of this neutralization effect encountered in the present investigation is shown in Fig. 18. The solid curve is taken from Fig. 12 for N_2^+ on aluminum at $\theta_i = 60°$. The unflagged symbols represent three points on this curve. The flagged symbols represent these same points after correction to the N_2 molecule using the largest probable value of $\Delta E = 1$ eV. Because the deviations from the curve are much less than the experimental repeatability for the present investigation, no corrections are made to the data for this effect.

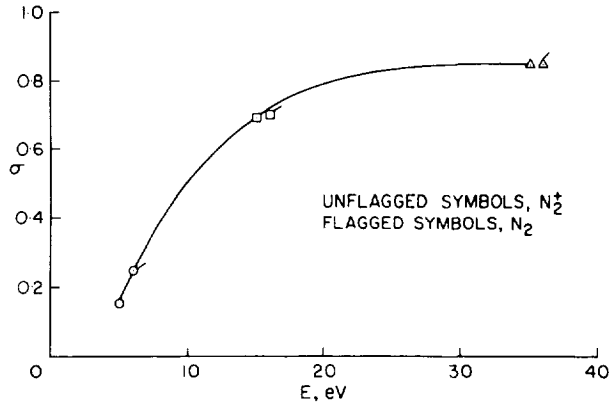

FIG. 18. Effect on σ of correction from N_2^+ to N_2: $\theta_i = 60°$.

Résumé—Accomodation de moment tangentiel et normal pour les conditions de satellite Terrestre. L'accomodation de moment a été déterminée expérimentalement pour les interactions de surface gazeuse simulant de manière pratique celles de satellites proches de la terre. Dans toute la gamme d'énergies gazeuses et d'angles d'incidence d'intérêt pour les conditions orbitales terrestres, deux composants de force ont été mesurés grâce à une micro-balance à vide pour déterminer les coefficients d'accomodation de moment tangentiel et normal pour les ions de nitrogène sur des surfaces d'aluminium de qualité technique. Pour ces conditions expérimentales, l'électrodynamique de neutralisation d'ions près de la surface, indique que les résultats pour les ions de nitrogène ne devraient être que peu différents de ceux s'appliquant aux molécules de nitrogène, lesquelles forment le plus grand composant de flux de moment pour les satellites près de la terre.

Les résultats expérimentaux ont indiqué que les coefficients d'accomodation de moment tangentiel et normal varient beaucoup avec l'énergie, tendant à être assez bien accomodés aux plus hautes énergies et devenant progressivement moins accomodés à mesure que l'énergie est réduite aux vitesses égales ou inférieures à celles de satellites terrestres. Les deux coefficients varient également grandement avec l'angle d'incidence, le moment normal devenant moins accomodé à mesure que l'angle d'incidence devient plus effleurant, alors que le moment tangentiel devient généralement plus complètement accomodé. Pour chaque coefficient de moment, une fonction de corrélation empirique a été obtenue qui se rapproche de très près des résultats expérimentaux sur les gammes d'énergies et d'angles d'incidence. La plupart des variations d'accomodation de moment observées avec l'énergie et l'angle d'incidence ont été qualitativement indiquées par un calcul utilisant un modèle tri-dimensionel qui simulait la surface cible par un potentiel d'attraction uni-dimensionel et par un potentiel d'attraction uni-dimensionel et par des réflecteurs sphériques durs.

Zusammenfassung—Normale und tangentiale Momentanpassung bei Erdsatellitbedingungen. Es wurde Momentanpassung für Gas-Oberflächenwechselwirkungen experimentell ermittelt, indem diese praktisch für Satelliten nahe der Erde nachgeahmt wurden. Für alle Stufen der Gasenergieen und Anstellwinkel, welche für Erdumlaufverhältnisse von Interesse sind, wurden zwei Kraftkomponenten mittels einer Vakuummikrowaage gemessen, um die normalen und tangentialen Momentanpassungskoeffizienten für Stickstoffionen auf Aluminiumoberflächen von technischer Qualität zu ermitteln. Die Elektrodynamik der Ionenneutralisierung nahe der Oberfläche während dieser experimentellen Verhältnisse zeigt, dass Ergebnisse für Stickstoffionen sich verhältnismässig wenig von denen für Stickstoffmoleküle unterscheiden dürften, welche die grösste Komponente des Impulsflusses für Satelliten nahe der Erde darstellen.

Die experimentellen Ergebnisse zeigten, dass normale und tangentiale Impulsanpassungskoeffizienten stark mit Energie variierten und dazu neigten, sich bei grösseren Energieen verhältnismässig gut anzupassen, dass sie sich aber fortschreitend mit Reduzierung der Energie auf und unter die Geschwindigkeiten von Erdsatelliten weniger günstig anpassten. Beide Koeffizienten variierten erheblich mit dem Anstellwinkel, wobei das Normalmoment sich schlechter anpasste, wenn der Anstellwinkel streifender wurde, während das tangentiale Moment im algemeinen mehr anpassungsfähig wurde. Es wurde für jeden Momentkoeffizienten eine empirische Korrelationsfunktion erhalten, welche den experimentellen Ergebnissen über den Energie- und Einfallwinkelstufen sehr nahe kam. Die meisten der mit Energie und Einfallwinkel beobachteten Variationen der Momentanpassung wurden qualitativ durch Berechnung angezeigt, welche ein dreidimensionales Modell benutzte, das die Targetoberfläche mit einem eindimensionalen Anziehungspotential und harten Kugelreflektoren nachahmte.